15.316 END-TO-END CALIBRATION OF NEXRAD DIFFERENTIAL REFLECTIVITY WITH METAL SPHERES[†]

Earle Williams*, Kenta Hood, Dave Smalley, and Michael Donovan
MIT Lincoln Laboratory

Valery Melnikov, Doug Forsyth, Dusan Zrnic, Don Burgess and Michael Douglas
National Severe Storms Laboratory

John Sandifer, Darcy Saxion, Olen Boydstun and Adam Heck
Radar Operations Center

Thomas Webster
Federal Aviation Administration

1. INTRODUCTION

This study is concerned with the absolute calibration of radar differential reflectivity, ZDR. By definition, ZDR = 10 log (ZH/ZV), where ZH and ZV are the reflectivity values at horizontal and vertical polarization, respectively. The name of the calibration game is symmetry between horizontal and vertical channels, and the accurate matching of all radar quantities that contribute to asymmetry (antenna gain, transmitted power, received power). A metal sphere is a 0 dB target for ZDR at a level of accuracy exceeding any expectation. The generally desired level of accuracy for ZDR is 0.1 dB (Sachidananda and Zrnic, 1987; Zrnic et al., 2010) and has come to be known as the "Holy Grail" in polarimetric radar work. Now that the NEXRAD radars in the US have been upgraded with dual pol capability, the 0.1 dB criterion is increasingly recognized as a formidable challenge to all calibration methods presently available.

Why should one be deeply concerned with this stringent 0.1 dB level of accuracy? In a word, because the measurement promise of dual pol methods benefits from it. This promise lies in two distinct areas: hydrometeor classification and the radar measurement of rainfall (Park et al., 2009). In certain Z-ZDR rainfall relationships, the ZDR dependence has a strong power law relation (Giangrande and Ryzhkov, 2008).

The end-to-end calibration of weather radar reflectivity with a metal sphere is widely known and long-practiced (e.g. Atlas and Mossop, 1960), but has developed a bad reputation in some quarters because of the perceived difficulty in its implementation. An important conclusion of this work is that this method is easily extended to differential reflectivity Z_{DR}, providing two key calibrations for the price of one, and that the difficulties of implementation are rather easily overcome by suitable planning and selection of favorable meteorological conditions for the measurements.

These calibration measurements discussed here show that the variability in the refractive index of atmospheric medium may set the ultimate limit on how accurately one can measure the Z_{DR} value of a metal sphere. The standard deviation of the measurement exceeds the long-desired 0.1 dB.

2. Z_{DR} CALIBRATION METHODS: PROS AND CONS

The practice of calibration in any scientific endeavor typically involves a well-known standard against which the measurements are compared. In physics, the standards for length, mass, and frequency, for example, are known to many decimal places. Frequency can now be measured to a few parts in 10^{14}, and is the most accurately known physical quantity. In polarimetric radar work, the desired accuracy of 0.1 dB for differential reflectivity stated in the introduction seems a modest goal in the context of physics standards. In reality, the identification of calibration standards as radar targets

* This work was sponsored by the Federal Aviation Administration under Air Force Contract No. FA8721-05-C-0002. Opinions, interpretations, conclusions, and recommendations are those of the authors and are not necessarily endorsed by the United States Government.

† Corresponding author address: Earle Williams, MIT Lincoln Laboratory, 244 Wood Street, Lexington, MA - 2420

in the atmosphere at the level of 0.1 dB is no simple task, but nevertheless, this criterion (0.2 % as a percentage) allows a clear separation between "true" calibration and pseudo calibration, as summarized in Table 1. A calibration method is considered "true" if the differential reflectivity of the target is known with certainty to 0.1 dB or better.

Table 1: Calibration Approaches for Differential Reflectivity

True Calibration Methods	Pseudo Calibration Methods
Metal spheres	Hydrometeor calibration
Vertically pointing "bird bath"	Z-Z_{DR} asymptote method
Sun pointing (receiver check only)	Natural ground clutter (metal towers)
NCAR Cross-pol power method	Clear-air targets (Bragg scatter)
Engineering approach (Zrnic *et al*. 2006)	Baron approach (Balaji *et al.*, 2012)
Drizzle	

The oldest and most widely utilized method for Z_{DR} calibration is the so-called "bird bath" method involving a vertical radar beam (Newell *et al*.,1957; Bringi and Chandrasekar, 2005). With the beam aligned with gravity, raindrops are expected to present circular cross sections to radar measurement, with residual intrinsic Z_{DR} less than 0.1 dB. Furthermore, any hydrometeor, liquid or solid, is expected to present balanced H and V cross sections at vertical incidence, so birdbath calibration checks can be done even in snow. The other attractive feature of this method is that it relies on the same volume target which is the object of general dual pol measurements. But a show-stopping shortcoming of this method for newly polarimetric NEXRAD radars is the design restriction against vertically pointing. This limitation provided substantial motivation for further work on the method with metal spheres.

The problem with use of naturally occurring hydrometeors for calibration, known as the asymptote method (ROC, personal communication), is best illustrated by Figure 1 showing the differential reflectivity of raindrops as a function of their mean diameters. Here it is seen that one needs to have drops smaller than 0.5 mm to reach the calibration tolerance of 0.1 dB. Disdrometer measurements in stratiform precipitation worldwide (Tokay and Short, 1996; Atlas *et al*., 1999; Campos and Zawadzki, 1999; Maki *et al*., 2000) all show appreciable numbers of raindrops in the 1 mm size range, and with inferred Z_{DR} values substantially greater than 0.1 dB.

The only practical way to achieve true calibration with naturally occurring hydrometeors at C-band and S-band is to focus on drizzle, whose microphysical origins are generally distinct from stratiform rain. The challenge here, particularly at the longer radar wavelengths, is to have sufficient reflectivity with drizzle, since reflectivity ~D^6, and drizzle drops are by definition (AMS Glossary, 2000) in the diameter range 200-500 μm, and according to Figure 1, characterized by Z_{DR} values less than 0.1 dB.

Currently competing for status as 'true' calibration is the Bragg scatter mechanism from isotropic turbulence (Melnikov *et al*., 2011). Despite signs of success here in recent trials with newly polarimetric NEXRAD radars, we have relegated this approach to the pseudo calibration category because (1) there is currently no guarantee that boundary layer turbulence is isotropic as the level of 0.1 dB in Z_{DR} space, and (2) insects are well known to masquerade as Bragg scatter, particularly in summertime, and their differential reflectivity can depart markedly from 0.1 dB.

Ground targets (corner reflectors, metal towers, stable ground clutter) can be used as radar calibration checks (Rinehart, 1978; Silberstein et al., 2008), but these procedures are definitely in the pseudo-calibration category because the absolute cross sections are not known, and furthermore cannot be guaranteed to be stable over time. In the context of Z_{DR} measurements, it is conceivable that metal struts and attachments on the scale of the radar wavelength are sufficiently randomly oriented that the Z_{DR} value will be close to zero, but 'close' would need to be checked by a radar with absolute Z_{DR} calibration.

The cross-pol calibration method (Hubbert *et al*., 2003; Hubbert *et al*., 2011) depends in part on the receiver calibration based on matched natural H and V emission from the Sun. End-to-end calibration involving both the radar transmitter and receiver is achieved by observations of natural ground clutter. This calibration method is a viable alternative when using a fast, alternating H and V transmitting radar. However, this technique is difficult to implement on the NEXRAD radars due to the simultaneous transmission of H and V polarizations and the results of this method have yet to be published. The

refractive index variability that will be shown to dominate the pulse-to-pulse variability of returns from the metal sphere will also plague the cross-pol calibration.

The calibration of radar reflectivity with balloon-tethered metal spheres, though well spelled out in theory and with some documented success (Atlas and Mossop, 1960), has developed a bad reputation in practice. Anyone who has attempted this procedure in the presence of winds greater than a few meters per second knows why. In such conditions, the stabilization of the spherical target in the pulse resolution volume of the radar (see Figure 2) at relatively close range (a few km or less) is difficult. Finding a strong and stable return from the sphere against the sometimes formidable ground clutter is seldom achieved. These problems can be easily overcome, however, by a patient, organized procedure, as will be demonstrated in the present study.

3. METAL SPHERES AND THEIR DEPLOYMENT FOR CALIBRATION

The scattering of electromagnetic waves by metal spheres is a heavily-travelled subject and the scattering cross sections versus wavelength are well known. Figure 3 shows the normalized cross sections as a function of the non-dimensional scattering parameter $2\pi a/\lambda$ over three scattering regimes: the complicated Mie regime bounded by the Rayleigh regime on the left and the geometrical optics regime on the right. The scattering parameter values for the 6" and 12" diameter spheres are clearly marked with vertical lines. At the S-band wavelength considered for the measurements here, one is not completely out of the oscillatory Mie regime, so some important corrections to the πa^2 prediction from geometrical optics when $2\pi a/\lambda >> 1$ are required.

Spheres with two distinct diameters were used for the calibration measurements so as to provide a more rigorous test of predictions. Table 2 summarizes information on the two spheres, including specifications on sphericity, which provide upper bounds on differential reflectivity. In both cases, these Z_{DR} estimates are below the goal of 0.1 dB, and can be considered perfect spheres. We avoided the less expensive calibration spheres consisting of two screw-together hemispheres out of concern for possible departures from spherical symmetry.

Table 2: Specifications of metal calibration spheres

Diam.	Composition	Manufacturer	Cost	Sphericity	Maximum Z_{DR}
6"	Aluminum	Century Metal Spinning Co.	$400	0.005" in 6"	< 0.007 dB
12"	Aluminum	Trimillenium Corp.	$722	0.5%	<0.043 dB

The metal sphere was securely tied with a short piece of kite cord to the base of a helium-filled neoprene weather balloon. The balloon, inflated to a diameter of 1-2 meters, was tethered with kite cord and lofted to an altitude in the range of 100-160 meters with a hand-held kite winder. Figure 4 shows the typical geometry of the deployment. In this configuration, one has two pendulums at work, both of which were manifest in the radar observations as will be described in Section 4.

For nighttime work, a spotlight was procured following FAA requirements that elevated targets near airports be illuminated.

The theory we have used for the calibration of radar reflectivity (dBZ) with metal spheres (Russell *et al*., 2010) is based on the well known theoretical results for the volume reflectivity (often denoted by η, and with units of area per unit volume) of spheres in two wavelength limits: (1) the Rayleigh regime ($\lambda >> D$), for which

$$\eta = \frac{\pi^5 |k|^5 Z}{\lambda^4} \left(\frac{m^2}{m^3}\right), \quad (1)$$

and (2) the geometrical optics regime ($\lambda << D$) in which the radar cross section σ is simply the physical cross section ($\sigma = \pi r^2$) and the effective volume reflectivity is that cross section shared over the radar pulse resolution volume (PRV)

$$\eta = \frac{\sigma}{PRV} \left(\frac{m^2}{m^3}\right), \quad (2)$$

Where

$$PRV = \frac{\pi \theta \varphi h R^2}{8} (m^3). \quad (3)$$

θ is the horizontal 3 dB beam width, φ is the vertical beam width, h is the radar pulse length, and R is the range between radar and target. Figure 2 illustrates the metal sphere centered in the pulse resolution volume of the radar. Probert Jones (1962) noted that the pulse resolution described here is not uniformly illuminated by the radar beam when calibration for a

volume target is being considered, thereby requiring a correction to the results for a point target of +1.5 dB.

Equating the two formulae for volume reflectivity, (1) and (2) produces an expression for the effective reflectivity (Z) of a calibration sphere within the PRV that is dependent on radar range:

$$Z = \frac{8\lambda^4}{\theta\varphi h\pi^5|k|^5}\frac{r^2}{R^2}\left(\frac{mm^6}{m^3}\right). \quad (4)$$

The numbers used in the calculations are as follows:

r = 7.62 cm (6" sphere)
r = 15.2 cm (12" sphere)
λ = 11.08 cm
θ = φ = 0.95 deg = 1.66 x 10^{-2} rad
h = 1.50 μs
$|k|^2$ = 0.93
R = 3400 m

When (4) is corrected for both Probert-Jones (1962) and for the departures in Mie scattering for both 6" (1.1 dB) and 12" (0.2 dB) metal spheres shown graphically in Figure 3, the expected values for reflectivity Z of both spheres can be computed, and these values (42.7 dB for 6" sphere; 50.0 dBZ for 12" sphere) appear in Table 3. The predicted value of Z_{DR}, following the manufacturer's data on the metal spheres, is clearly 0 dB.

Table 3: Summary of measured values on two calibration spheres

Sphere Size	Elev. (deg)	Predicted Z (dBZ)	Measured Z (dBZ)	Std. Dev. Z (dB)	Predicted Z_{DR} (dB)	Measured Z_{DR} (dB)	Std. Dev. Z_{DR} (dB)
6"	1.36	42.7	42.5	0.47	0	-0.56	0.25
12"	1.23	50.0	46.7	0.36	0	-0.52	0.20

4. RADAR PROCESSING

The computations performed for this work are consistent with the algorithms in the NEXRAD ORDA for processing raw time-series data. Processing methods for both the horizontal polarization and vertical polarization are the same and the discussion will touch on how to process power and reflectivity in a general sense instead of specifically for either polarization.

Received power P is computed as the mean of the magnitude squared for the time-series data as shown in (5), where M is the number of samples used in the computation.

$$P_{H,V}(mW) = \frac{1}{M}\sum_1^M |I + Q|^2 \quad (5)$$

While received power is useful, reflectivity in dBZ is used to represent the intensity of the observed phenomena in a weather radar system. Reflectivity is computed as

$$Z_{H,V}(dBZ) = 10\log_{10}\left(\frac{(P_{H,V} - N_{H,V})}{N_{H,V}}\right) + \quad 20\log_{10} r + l + dBZ_0, \quad (6)$$

where N is noise power in mW, r is range in kilometers, l is the correction term for atmospheric losses based on elevation angle and range, and dBZ_0 is the calibration reflectivity term. At S-band, the atmospheric losses are negligible for short ranges so the correction term was not used. The calibration reflectivity term is the minimum detectable dBZ value at a range of 1 km and is provided in the recorded data header.

Differential reflectivity is computed as shown in (7).

$$Z_{DR}(dB) = 10\log_{10}\left(\frac{P_H - N_H}{P_V - N_V}\right) \quad (7)$$

5. KOUN RADAR MEASUREMENTS

The selection of location for sphere deployment in calibration measurements is dictated by the need to be in the far field of the radar but not so close that ground clutter dominates and not so far that the return from the spherical target (diminishing as the fourth power of the radar range) becomes unimportant. Toward finding a suitable site near the KOUN radar, ground clutter maps were examined in comparison with street maps of Norman, Oklahoma to enable vehicle access. The combined virtues of relatively weak clutter and ease of access were achieved with a large, flat field ~3 km east of the radar site.

A theodolite was set up on the KOUN radar tower directly below the antenna, and its pointing directions established to a few tenths of a degree by pointing at towers with known GPS coordinates. Once the tethered balloon was in its final position, the theodolite operator was able to find and report its location to the radar operator, who in turn located the metal sphere on the A-scope display.

Figure 5 shows the A-scope display with the 6" sphere deployed by balloon at a slant range of 3.4 km. The strongest return over this 14 km range

interval is associated with the calibration sphere (~42 dBZ), with a signal-to-clutter ratio approximately 15-25 dB higher relative to its surroundings.

Figure 6 shows time-series of simultaneous pulse-to-pulse measurements of Z_H , $Z_{V,}$ and Z_{DR} for a 10 second interval when the reflectivity returns were at a maximum, indicating the beam was centered on the sphere and maximum stability prevailed. Z_H and Z_V exhibit peak-to-peak variability of approximately 2-3 dB and peak-to-peak variations in Z_{DR} on the order of 1 dB.

Figure 7 shows a time-frequency spectral plot for the 6" sphere in which 128 pulse integrations were used. As expected for a tethered sphere, the mean radial velocity in this plot is zero but also evident is a low frequency variability (with periods on the order of 5-10 seconds) and a more consistent high frequency 'ripple', with a period on the order of one second. The former variability we associate with the highly damped pendulum motion of the balloon on the long tether. The latter variability is attributed to the pendulum motion of the sphere tied at the base of the balloon. For example, the simple pendulum formula for period $T = 2\pi\sqrt{(L/g)}$ gives a 1.3 second period with a length L of 42 cm. This is in reasonable agreement with the observations.

Figure 8 shows a one-dimensional Doppler spectrum, again with 128 pulse integrations. The 3 dB spectral width of the prominent maximum near 0 m/s radial velocity is only 0.2 m/s. Following the theory for the simple pendulum, the maximum azimuthal speed of oscillation of the sphere on this short string length L, and maximum angular swing α, is given by

$$\sqrt{gL(1-\cos\alpha)}, \qquad (8)$$

which for an angle of 10 degrees from the vertical would be a speed of 0.25 m/s. This estimate is also in reasonable agreement with these spectral observations.

The larger 12" diameter metal sphere was deployed on the same tether line, returned to the same altitude level, and was found quickly by KOUN radar operators in the A-scope display, shown in Figure 9. Here, the nominally 6 dB stronger cross section stands out more conspicuously (at the same radar range of 3.4 km) relative to the ground-clutter background than was the case for the 6" sphere, with a signal-to-clutter ratio of approximately 20-25 dB.

Figure 10 shows the time-series of Z_H , Z_V and Z_{DR} on a pulse-to-pulse basis for a ten-second interval when the return was maximized by the radar operators with attention to the real-time A-scope display. The peak-to-peak variability in both reflectivity returns are again in the range of 2-3 dB. Though Z_H and Z_V are clearly correlated, they are clearly not identical, and when the differential reflectivity is examined, the peak to peak variability there amounts again to about 1 dB, similar to the results for the 6" sphere (Figure 6).

The time-frequency spectral plot for the 12" sphere, for a 100 second period and with 128-pulse integration for the spectra, is shown in Figure 11. The high frequency 'ripple' is readily apparent, with a periodicity of ~1.5 sec, and is again attributed to the pendulum motion of the metal sphere suspended beneath the balloon. A more irregular variation with longer periodicity is attributed to the damped pendulum motion on of the balloon/sphere combination on the 150 meter tether line.

The final illustration of the behavior of the 12" sphere shows the integrated Doppler spectrum (Figure 12) with 128 pulse integration. The pronounced maximum associated with this point target stands nearly 80 dB above the 'background' and shows a narrow spectral width of 0.2 m/s.

All the results of the comparisons on the metal spheres are summarized in Table 3. This includes the theoretical estimates and the experimental measurements, with both pulse-to-pulse and with 128-sample integrations.

6. EVIDENCE FOR SYSTEMATIC NEGATIVE Z_{DR} OFFSETS IN PRESENT NEXRAD NETWORK

While the NEXRAD Radar Operations Center (ROC) explores options for developing robust, repeatable dual polarization calibration methods for the network, alternate anecdotal approaches are being used to assess network-wide calibration. The method involves identifying regions of light rain in a radar volume beneath the melting layer (by virtue of Z and Z_{DR} levels) to compare against the expected returns of light rain based on a large set of disdrometer DSDs from central Oklahoma. Most recent data discussed (ROC, personal communication) for April-June 2013 suggests about 40% of the network could be out of calibration to the 0.1 dB Z_{DR} standard. Some radar sites have been out of calibration to that standard for quite some time but

cannot address the issue due to lack of necessary rainfall (i.e. – out west). Independent of one's opinion on the merit of the method, the evidence suggests the need for rectifying the calibration uncertainty as soon as possible. Additional sphere calibrations might be found useful in this context.

7. DISCUSSION

The agreement on reflectivity between theory and measurement on the 6" metal sphere is excellent and amounts to a difference of only 0.2 dB. Figure 13 illustrates power as a function of range and time for the 6" sphere. The elevated power at the 15th range bin shows the sphere was centered well in range as power levels are approximately 20 dB down in the adjacent bins. The agreement for the 12" sphere between theory and measurement is substantially worse (~3 dB) but can readily be attributed to the sphere not being centered in the radar range bin. In Figure 14, it can be seen that the 12" sphere is nearing the far edge of the bin in range as the difference in power between the 15th and 16th range bins is approximately 10 dB.

The differences in agreement between the two spheres can be explained when the conditions of the experiment are better known. The location of the sphere tether was chosen such that under ideal conditions with no wind, the sphere would be in the center of the PRV in range. An adjustment in azimuth could be made at the radar to center the sphere azimuthally. During the data collection for the 12" sphere, there was a slight breeze from the west that caused the balloon to drift from the center of the PRV toward the far end of the PRV in range. At the time, it was unknown that this was the case so no corrections were made to move the tether closer to the radar to bring the sphere back to the center of the PRV. When the 6" sphere was raised aloft half an hour later, the breeze had ceased and the sphere was located in the center of the PRV, hence the excellent agreement between the theoretical and measured value of reflectivity.

The agreement between theory and experiment on Z_{DR} is substantially worse with a rather large deviation of approximately -0.5 dB from the expected value of 0 dB. One had reasonable confidence in the results because both spheres showed essentially the same deviation. We do not expect the lack of centering of the 12" sphere in range to have an effect onthe Z_{DR} value but only the Z value. At the time of the calibration measurement (October 2011), these large Z_{DR} offsets were quite surprising. However, in light of recent checks on Z_{DR} offsets at many sites of the newly configured WSR-88D network, this calibration measurement has greater credibility. In April 2013, ten radars were showing Z_{DR} offsets exceeding -0.2 dB and in May 2013, 25 radars showed such offsets.

The considerable pulse-to-pulse variability of Z_{DR} in the measurements on both spheres (Figures 6 and 10) has been a major source of puzzlement since the day of the measurements. Going in to the field experiment, we had expectations for a more stable response, simply because the paths taken by H and V polarized waves are identical, the radar transmission is synchronous, and the sphere is a symmetrical target. The initial hypothesis for the observed variability involved either multiple targets (metal sphere plus neoprene balloon) or multiple paths (direct beam plus sidelobe contribution). The first possibility was ruled out by measurements of the balloon alone, in exactly the same measurement geometry as Figure 2, but without the metal sphere attached, showing that the balloon was at least 20 dB down relative to the return from the sphere. The second possibility is unlikely because the variability of the pulse-to-pulse returns (Figures 6 and 10) is substantially less than the predictions for multiple Rayleigh targets (Marshall and Hitschfeld, 1953). Further evidence for a single scatterer is the very narrow spectral width of the metal sphere, in both cases (Figures 8 and 12), measured at 0.2 m/s, which in turn is consistent with simple harmonic pendulum motion of the sphere at the base of the balloon. This speed is substantially less than the measured spectral width at horizontal incidence on weather targets involving multiple scatterers.

Further consideration of this problem leads to evidence that the variations in the atmospheric medium are possibly responsible for the pulse-to-pulse variations in Z_{DR} for the metal spheres. The mean effect of the atmospheric medium on EM wave propagation is a slowing of the speed of light by 3 parts in 10,000 relative to propagation in vacuum (Bean and Dutton, 1966). The atmospheric medium is largely non-dispersive and so measurements at optical frequencies (where pulse lengths can be made as short as one picosecond, or 0.3 mm in space) are a useful guide for microwave behavior. Owing to natural space-time variability in the refractive index (due to both temperature and humidity variability), one has jitter in the arrival times of light pulses propagating over long paths (6800 meters in the round-trip radar path to the metal sphere, Figure 2)

through the atmosphere that can amount to a significant fraction of an S-band radar wavelength. For example, Blasej et al. (2011) studied the deviation (jitter) in propagation distances of short light pulses (λ = 532 nm; PW=8 ps) over a horizontal distance of 4300 m through the lower atmosphere and found a 2-sigma spread of 2.8 mm. The peak-to-peak jitter with 1 kHz sampling was about 8 mm over the 4300 m path.

Assuming these jitter lengths apply at S-band frequencies over a similar path length as shown in Figure 4, a jitter length of 2.8 mm is 2.5% of a radar wavelength (11.08 cm), and would introduce a phase shift of 2.5% x 360 = 9.0 degrees. This could serve to shift the phase of the H and the V wave trains along the radar beam, and introduce a variation in Z_{DR} of order

$$\Delta Z_{DR} = 10 \log \left[\frac{\sin 90}{\sin 99.0} \right]^2 = 0.11\ dB, \qquad (9)$$

an amount comparable to the standard deviation in the Z_{DR} time-series for a metal sphere (Figures 6 and 10). For the peak-to-peak jitter value of 8 mm in range, that would be 7.2% of a radar wavelength, or a maximum possible phase shift of 7.2 % x 360 = 25.9 degrees between the H and V channels. The corresponding variation in Z_{DR} would be

$$\Delta Z_{DR} = 10 \log \left[\frac{\sin 90}{\sin 115.9} \right]^2 = 0.92\ dB. \qquad (10)$$

This prediction is likewise in reasonable agreement with the peak-to-peak variation of Z_{DR} in the measurements shown in Figures 6 and 10.

One possible objection to the foregoing interpretation for Z_{DR} variability is that the atmospheric propagation paths for H and V waves are identical. However, the medium is anisotropic, and the evidence for that is the variable Z_{DR} response of Bragg scattering (Melnikov et al., 2011), a mechanism whose underlying physics is the same: spatial variability in refractive index.

Another possible alternative explanation for the variability in Z_{DR} is one based on multipath interference. The direct path is along the center of the radar beam but other paths may involve off-beam-center forward scattering from the ground, to the sphere. The phases for the two scattered components are expected to be different and uncorrelated. In this sense, this explanation for the fluctuations in ZDR is the same as the one described previously.

8. CONCLUSIONS

The measurement of differential reflectivity on 6" and 12" metal spheres with the KOUN WSR-88D radar in October 2012 showed negative bias of -0.56 and -0.52 dB respectively, for both spheres. The offset is large in comparison to the desired accuracy of 0.1 dB. However, the measurements also suggest that the natural variability of the atmospheric medium will set the ultimate limit on the accuracy with which Z_{DR} can be determined by measurements on calibration spheres.

ACKNOWLEDGEMENTS

We thank Jim Metcalf for a recent reminder about early work on the polarimetric radar calibration by Reg Newell and Speed Geotis. Discussion with J. Blazej has benefitted this work.

REFERENCES

Atlas, D. and S.C. Mossop, 1960: Calibration of a weather radar by using a standard target. *Bull. Am. Met. Soc*., **41**, 377-382.

Atlas, D., C.W. Ulbrich, F.D. Marks, Jr., E. Amitai, and C.R. Williams, 1999: Systematic variation of drop size and radar-rainfall relations, *J. Geophys. Res.*, **104**, 6155-6169.

Balaji, M.S., J.R. Ellis, W.H. Walker, D.R. Cartwright, J.H. Lee, J.H. Romines, 2012: An engineering illustration of the dual polarization upgrade for the WSR-88D, *Proceedings of the Seventh European Conference on Radar in Meteorology and Hydrology, ERAD 2012*, pp. 1-6, Toulouse, France, June 2012.

Bean, B.R. and E.J. Dutton, 1966: *Radio Meteorology*, National Bureau of Standards Monograph 92, U.S. Government Printing Office, Washington, D.C.

Bringi, V.N. and V. Chandrasekar, 2005: *Polarimetric Doppler Weather Radar: Principles and Applications*, Cambridge University Press.

Blazej, J., I. Prochazka and L. Kral, 2011: Picosecond laser pulse propagation delay fluctuation through atmosphere. *Proc. of SPIE*, **7924**, 79240A-1.

Campos, E. and I. Zawadzki, 1999: Instrumental uncertainties in Z-R relations, *J. Appl. Met.*, **39**, 1088-1102.

Giangrande, S.E. and A.V. Ryzhkov, 2008: Estimation of rainfall based on the results of polarimetric echo classification. *J. Atmos. Ocean Tech.*, **47**, 2445-2462.

Glossary of Meteorology, Ed. T.S. Glickman, American Meteorological Society, Boston, 2000, 855 pp.

Hubbert, J.C., V.N. Bringi and D. Brunkow, 2003: Studies of the polarimetric covariance matrix. Part 1: Calibration Methodology, *J. Atmos. Ocean Tech.*, **20**, 696-706.

Hubbert, J.C., M. Dixon, A. Heck, S. Ellis, V. Chandrasekar, P. Kennedy, D. Brunkow, R. Ice, and D. Saxion, 2011: Zdr calibration and simultaneous horizontal and vertical transmit operation. *Proc. American Meteorological Society's 35th International Radar Conference, Pittsburg, PA*.

Maki, M., T.D. Keenan, Y. Sasaki and K. Nakamura, 2001: Characteristics of the tropical size distribution in tropical continental squall lines observed in Darwin, Australia. *J. Appl. Meteorol.*, **40**, 1393-1412.

Marshall, J.S. and W. Hitschfeld, 1953: The interpretation of the fluctuating echo for randomly distributed scatterers, Part I, *Can. J. Phys.*, 962-994.

Melnikov, V.M., R.J. Doviak, D.S. Zrnic and D.J. Stensrud, 2011: Mapping Bragg scatter with a polarimetric WSR-88D. *J. Atmos. Ocean Tech.*, **28**, 1273-1285.

Newell, R.E., S.G. Geotis and A. Fleisher, 1957: The shape of rain and snow at microwavelengths. *MIT Department of Meteorology, Research Report No. 28, Contract No. DA-36-039 SC-71136*, U.S. Army Signal Engineering Laboratories, Ft. Monmouth, New Jersey, September 1957.

Park, H., A.V. Ryzhkov, D.S. Zrnic, and K-E. Kim, 2009: The Hydrometeor Classification Algorithm for the Polarimetric WSR-88D: Description and Application to an MCS. *Wea. Forecasting*, **24**, 730–748.

Probert-Jones, R.F., 1962: The radar equation in meteorology, *Quart. J. Roy. Met. Soc.*, **88**, 485-495.

Prochazka, I., L. Kral and J. Blazej, 2010: Picosecond laser pulse distortion by propagation through a turbulent atmosphere. *Chapter 19 in Coherence and Ultrashort Pulse Laser Emission, Ed.*, F. J. Duarte, ISBN 978-953-307-242-5, Published: December 30, 2010.

Rinehart, R.E., 1978: On the use of ground return targets for radar reflectivity calibration checks. *J. Appl. Met.*, **17**, 1342-1350.

Russell, B., E.R. Williams, M. Gosset, F. Cazanave, L. Descroix, N. Guy, T. Lebel, A. Ali, F. Metayer and G. Quantin, 2010: Radar/rain-gauge comparisons on squall lines in Niamey, Niger for the AMMA. *Quart. J. Roy. Met. Soc.*, **136**, 289-303.

Sachidananda, M. and D.S. Zrnic, 1987: Rain rate estimates from differential polarization measurements. *J. Atmost. Ocean. Tech.*, **4**, 588-598.

Silberstein, D.S., D.B. Wolff, D.A. Marks, D. Atlas, and J.L. Pippitt, 2008: Ground clutter as a monitor of

radar stability at Kwajalein, RMI. *J. Atmos. Ocean. Tech.*, **25**, 2037-2045.

Stratmann, J.A., D. Atlas, J.H. Richter and D.R. Jensen, 1971: Sensitivity calibration of a dual-beam vertically pointing FW-CW radar. *J. Appl. Meteor.*, **10**, 1260-1265.

Teschl, F., W.L. Randeu, M. Schönhuber, and R. Teschl, 2008: Simulation of polarimetric radar variables in rain at S-, C-, and X-band wavelengths. *Adv. Geosci.*, **16**, 27-32.

Tokay, A. and D.A. Short, 1996: Evidence from tropical raindrop spectra of the origin of rain from stratiform versus convective clouds. *J. Appl. Met.*, **35**, 355-371.

Zrnić , D.S., V.M. Melnikov and J.K.Carter, 2006: Calibrating differential reflectivity on the WSR-88D. *J. Atmos. Ocean. Tech.*, **23**, 944-951.

Zrnić, D., R. Doviak, G. Zhang and A. Ryzhkov, 2010: Bias in differential reflectivity due to cross coupling through the radiation patterns of polarimetric weather radars. *J. Atmos. Ocean. Tech.*, **27**, 1624-1637.

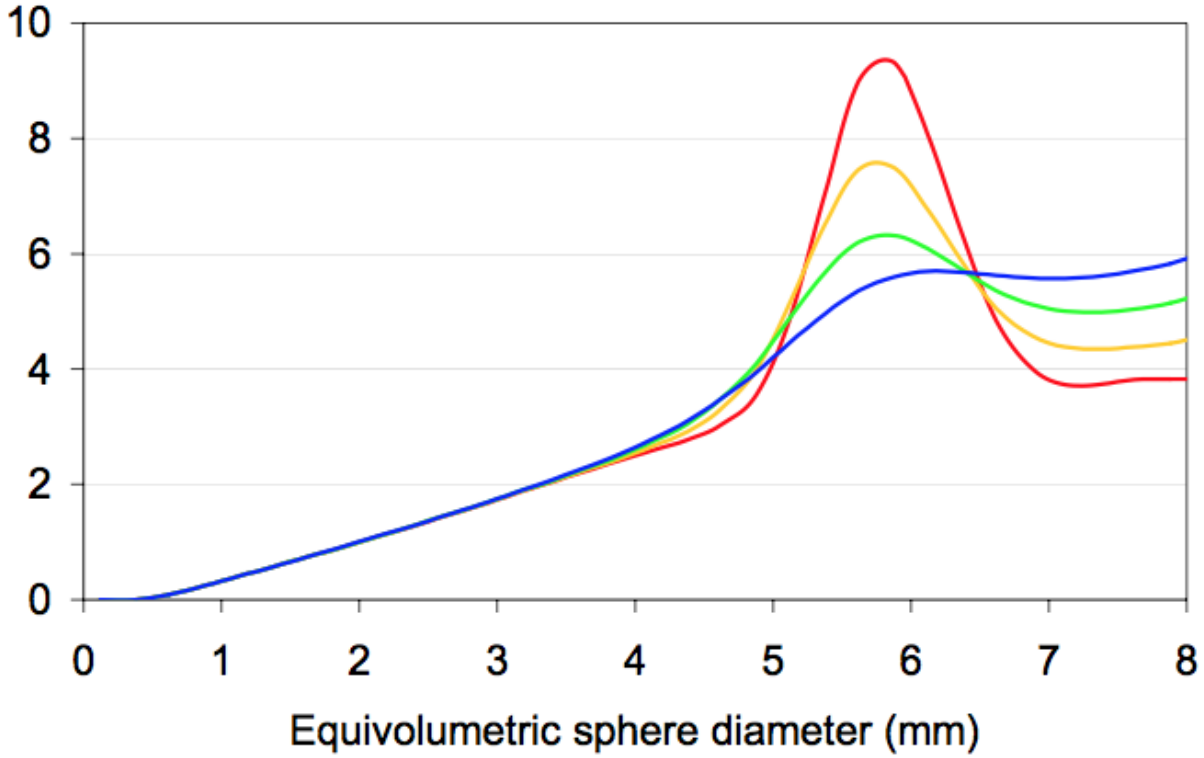

Figure 1,. Differential reflectivity for individual raindrops versus their mean volumetric diameters (from Teschl *et al*., 2008).

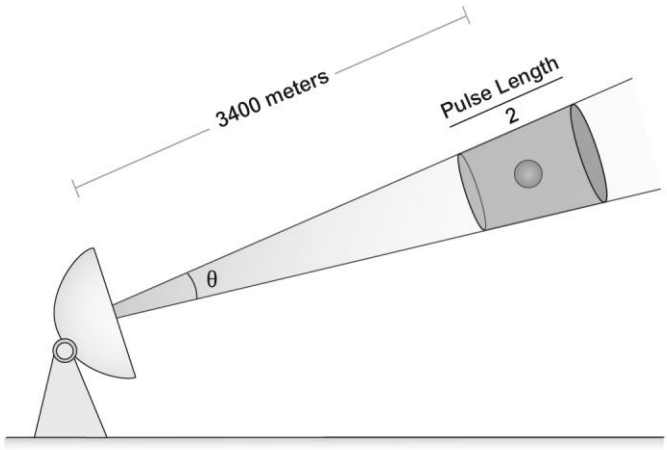

Figure 2. Illustration of radar observation of a metal sphere centered in the pulse resolution volume.

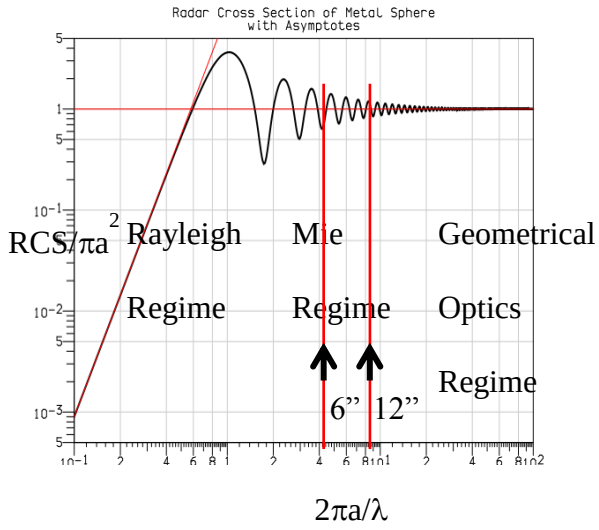

Figure 3. Radar cross sections of metal spheres (normalized to their geometrical cross sections) as a function of the non-dimensional scattering parameter 2πa/λ. The three characteristic scattering regimes (Rayleigh, Mie and geometrical optics) are marked. Vertical lines associated with the 6” and 12” diameter metal spheres are also shown.

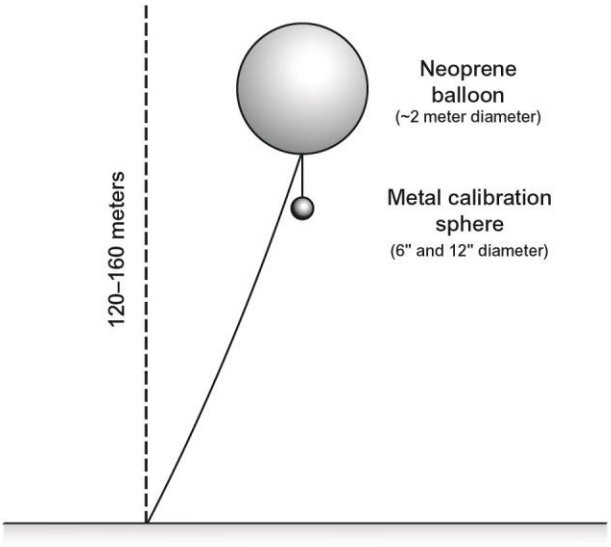

Figure 4. Illustration of the calibration sphere suspended from the tethered neoprene balloon for viewing by the KOUN radar.

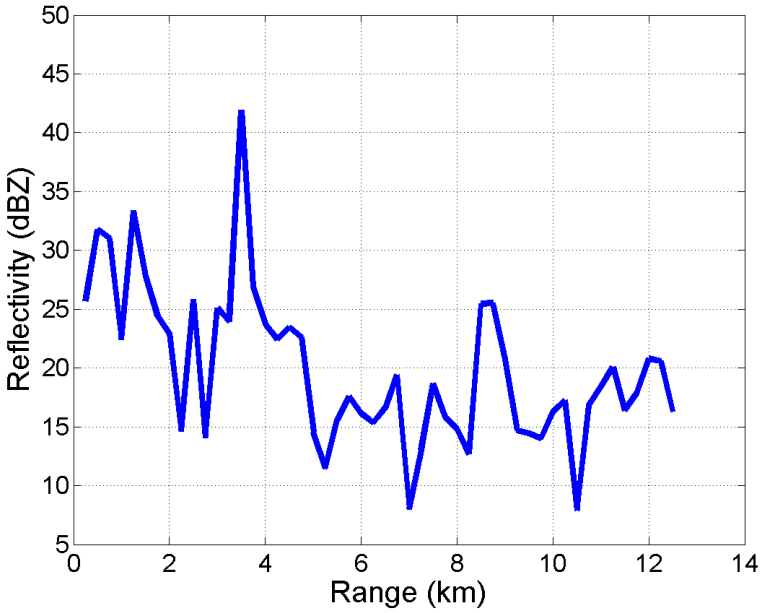

Figure 5. A-scope display for the KOUN radar aimed at the 6" diameter calibration sphere. This return predominates at a range of 3.4 km, and with an intensity of 42 dBZ. The SNR for the metal sphere target is typically 15-25 dB.

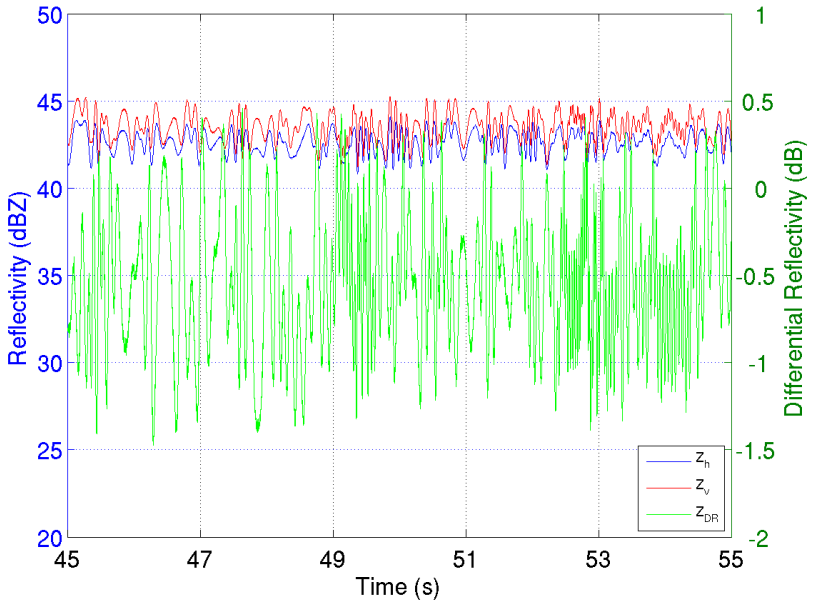

Figure 6. Pulse-to-pulse time-series of Z_H , Z_V and Z_{DR} at the range bin containing the 6" calibration sphere for a 10 second interval.

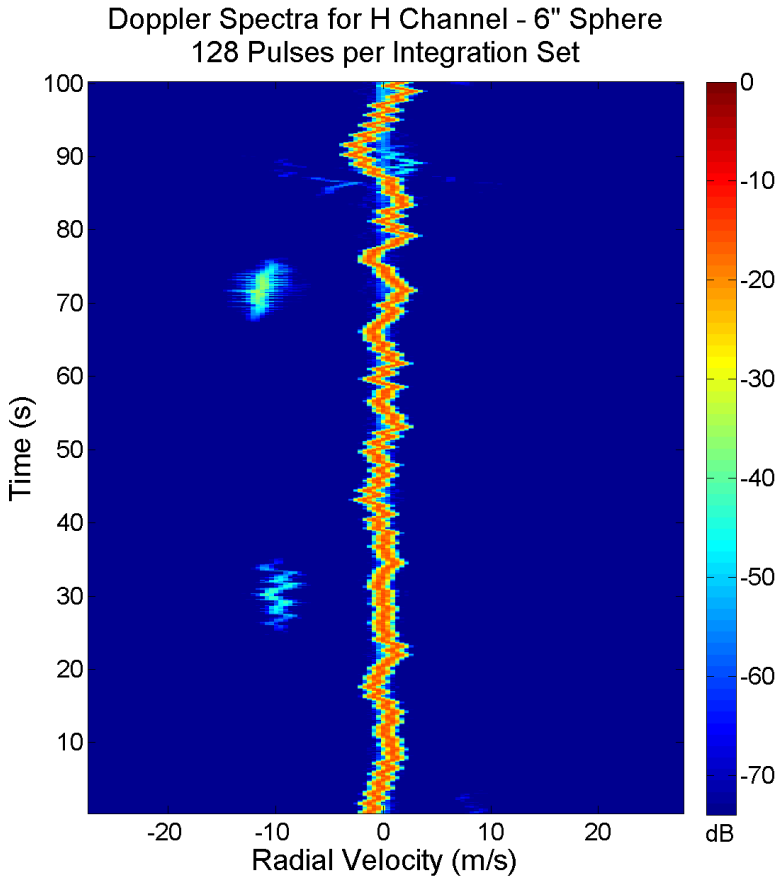

Figure 7. Time-frequency spectral plot for 100 seconds of radar viewing of the 6" metal sphere. 128-pulse integration is implemented here.

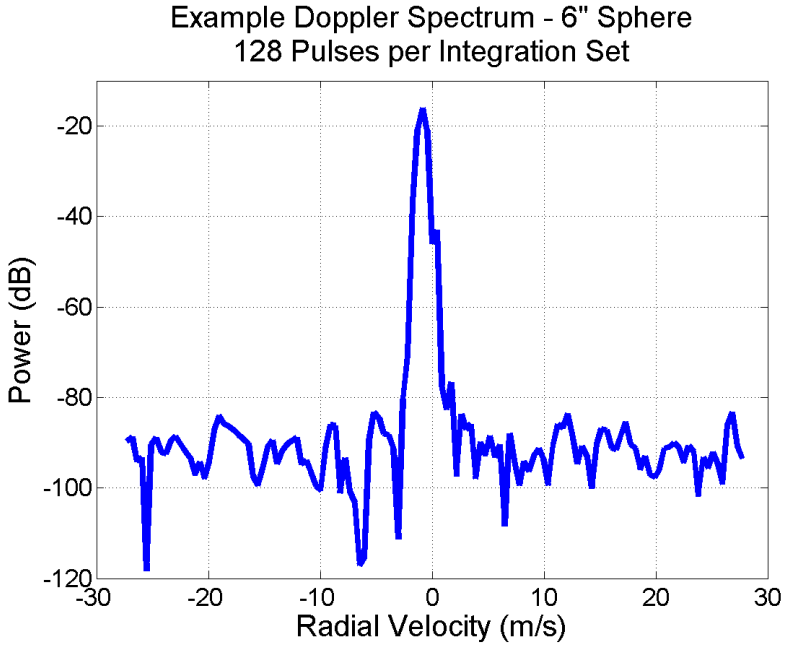

Figure 8. One-dimensional Doppler spectrum on the 6” metal sphere, with 128 pulse integration. The 3 dB standard deviation of Doppler velocity is 0.2 m/s.

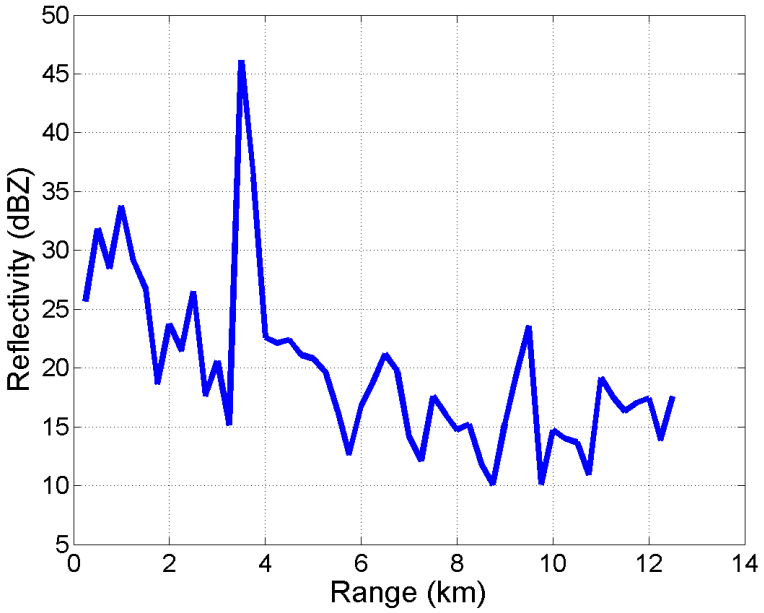

Figure 9. A-scope display for the KOUN radar aimed at the 12” diameter calibration sphere. This return predominates at a range of 3.4 km, and with an intensity of 46 dBZ. The SNR for the metal sphere target is typically 20-25 dB.

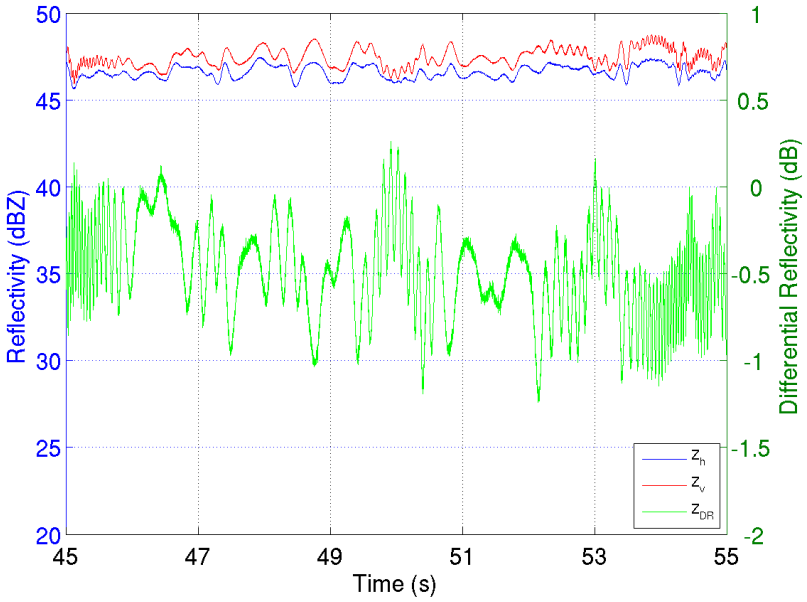

Figure 10. Pulse-to-pulse time-series of Z_H , Z_V and Z_{DR} at the range bin containing the 12” diameter calibration sphere for a 10 second interval.

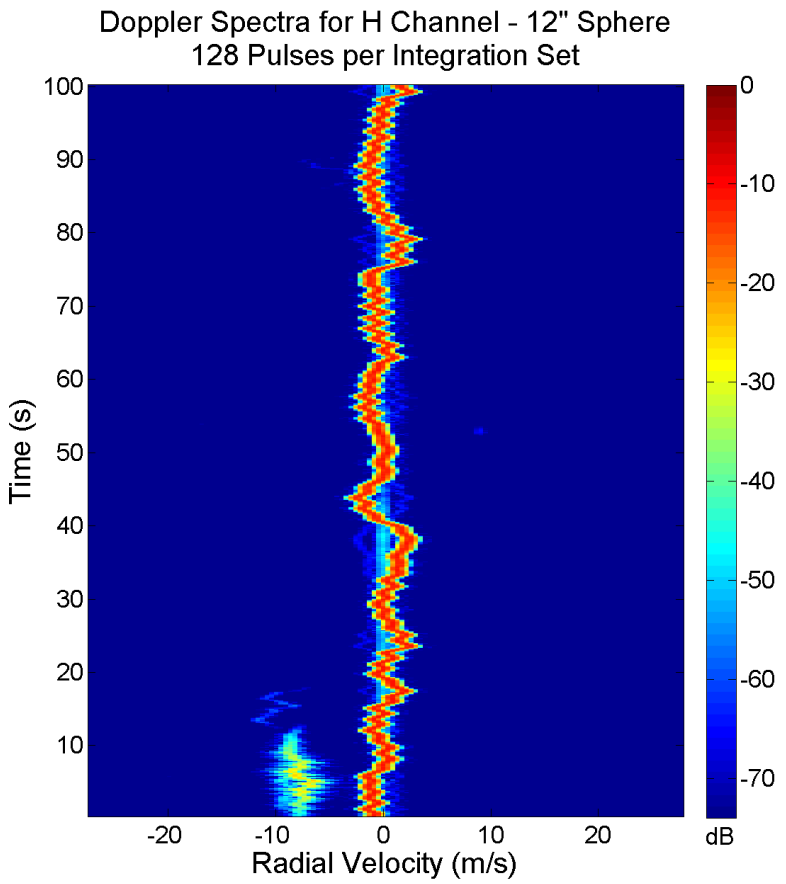

Figure 11. Time-frequency spectral plot for 100 seconds of radar viewing of the 12” diameter metal sphere. 128-pulse integration is implemented here.

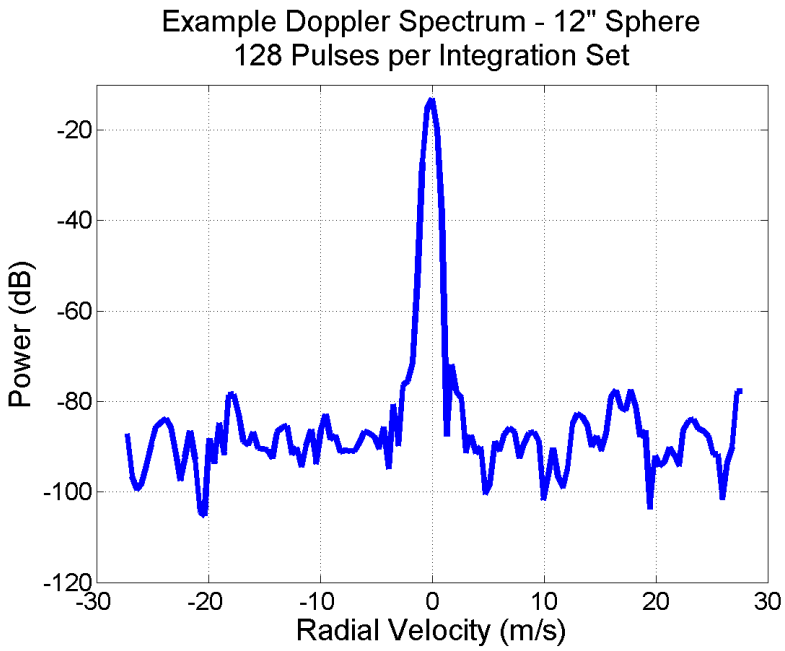

Figure 12. One-dimensional Doppler spectrum on the 12" diameter metal sphere, with 128 pulse integration. The 3 dB standard deviation of Doppler velocity is 0.2 m/s.

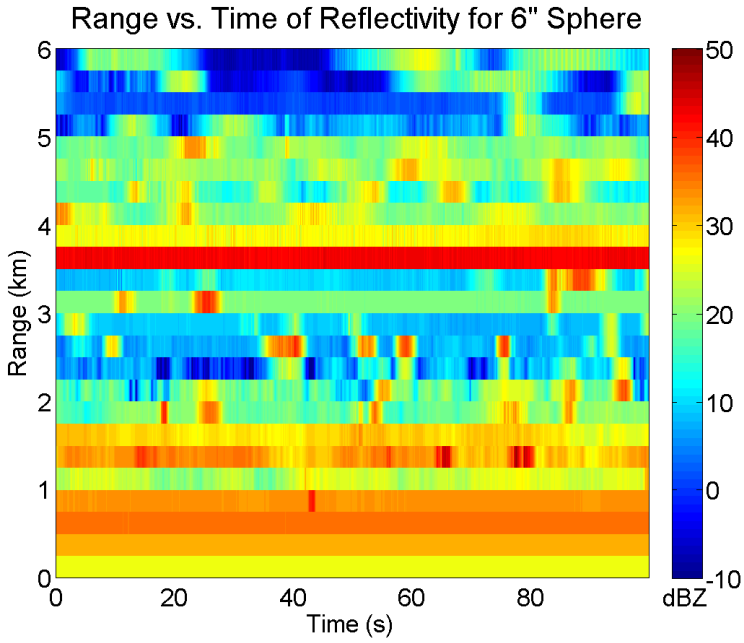

Figure 13. Power as a function of range and time for the 6" sphere. The location of the sphere in range can easily be discerned from the plot and the high signal-to-clutter ratio shows good centering in range with the PRV.

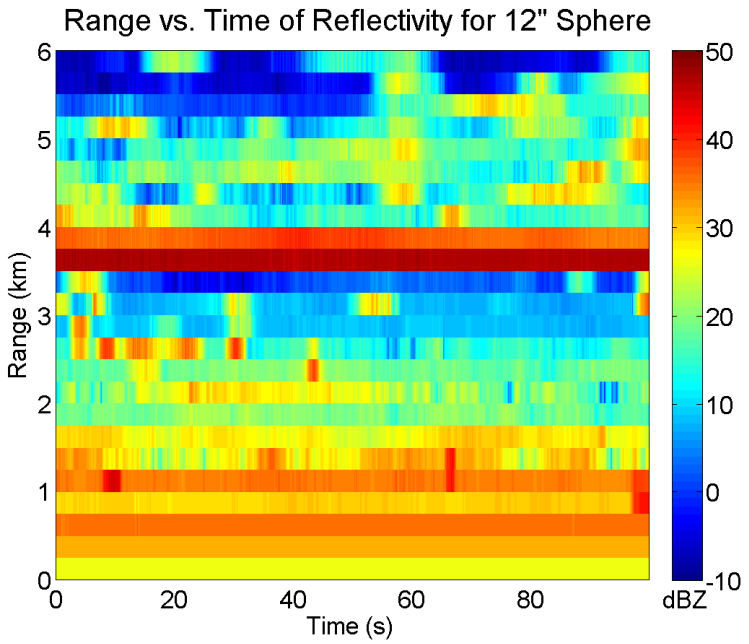

Figure 14. Power as a function of range and time for the 12” sphere. The location of the in range and nearing the far edge of the PRV.sphere in range can be seen but one can easily observe the sphere is not centered in range and nearing the far edge of the PRV.